ARTICLE OPEN

Check for updates

Demonstration of universal control between non-interacting qubits using the Quantum Zeno effect

E. Blumenthal[1]✉, C. Mor[1], A. A. Diringer[1], L. S. Martin[2], P. Lewalle[3,4], D. Burgarth[5], K. B. Whaley[3,4] and S. Hacohen-Gourgy[1]

The Zeno effect occurs in quantum systems when a very strong measurement is applied, which can alter the dynamics in non-trivial ways. Despite being dissipative, the dynamics stay coherent within any degenerate subspaces of the measurement. Here we show that such a measurement can turn a single-qubit operation into a two- or multi-qubit entangling gate, even in a non-interacting system. We demonstrate this gate between two effectively non-interacting transmon qubits. Our Zeno gate works by imparting a geometric phase on the system, conditioned on it lying within a particular non-local subspace. These results show how universality can be generated not only by coherent interactions as is typically employed in quantum information platforms, but also by Zeno measurements.

npj Quantum Information (2022)8:88 ; https://doi.org/10.1038/s41534-022-00594-4

INTRODUCTION

Control of quantum systems can be divided into two distinct schemes, coherent and incoherent control. Coherent control is achieved by application of control Hamiltonians to evoke deterministic time evolution. In contrast, incoherent control is based on non-deterministic measurement outcomes to prepare the system for the desired state. The two schemes may complement each other to enrich quantum control[1–8]. On the boundary between the two schemes lies the quantum Zeno effect, in which frequent measurements effectively freeze the system dynamics, holding the system at an eigenstate of the measurement observable. A more precise description shows that measurements divide the Hilbert space into subspaces with distinct eigenvalues of the measured observable, and give rise to 'Zeno dynamics' within each[9]. Transitions between subspaces are suppressed by measurement, but the evolution inside each subspace is completely coherent. In particular, previous work has shown that Zeno dynamics can theoretically transform a trivial (e.g., non-interacting with local control only) quantum system into one with universal control within the Zeno subspace[10] and several state entangling schemes have been proposed[11–13].

In this letter we show an explicit construction of such universal control, and demonstrate it in a circuit QED system[14]. Our construction performs in a single operation, an N-Control-phase gate on N qubits, where the last qubit is required to have only one extra level, i.e., it is a qutrit. We refer to this as a Zeno gate. Specifically, we demonstrate the gate between two non-interacting transmon qubits[15]. This work is distinct from other measurement based methods that prepare entangled states[5,16,17], in that the dynamics here are coherent, deterministic, and allow for universality.

Technically our experimental system has a resonator induced interaction, which can yield a high fidelity gate (RIP-gate)[18,19]. We actively cancel these interactions to make our system effectively non-interacting. We can then demonstrate dynamics due to the Zeno effect alone. Our purpose is to show how universality can be switched on and off just by looking at a single level within a quantum system.

The Zeno dynamics we explore here rely on local operations together with non-local projections. Locally driving one transition for a full 2π rotation imparts a geometric phase of π on the initial state. Adding rapid projections blocks transitions between the Zeno subspaces defined by the projector, and allows phase accumulation only for certain states. Choosing an appropriate non-local projector conditions the resulting phase on the state of both qubits and thereby leads to entanglement. This process is similar to entangling operations based on Rydberg blockade with neutral atoms[20,21] in the sense that a certain non-local state can not be reached by the system. The main difference is that while the Rydberg blockade is a result of strong coherent interactions[22], we use incoherent measurements to perform the Zeno block.

Consider first an ideal qutrit-qubit system and infinitely rapid projections, where the qutrit $|f\rangle$ level is an auxiliary state. We apply a Rabi drive of frequency Ω_R between $|e\rangle$ and $|f\rangle$, and at the same time apply rapid projective measurements of the projector $P = \mathbb{1} - |fe\rangle\langle fe|$ (as depicted in Fig. 1b). Note that throughout this paper, except if explicitly subscripted, the state of the qutrit is denoted to the left of the state of the qubit. In the limit of infinitely rapid projections the Hamiltonian reads[9]

$$\begin{aligned} H_{\text{Zeno}} &= PHP \\ &= i\hbar\tfrac{\Omega_R}{2} P \underbrace{(|e\rangle\langle f| - |f\rangle\langle e|)}_{\text{qutrit}} \otimes \underbrace{(|g\rangle\langle g| + |e\rangle\langle e|)}_{\text{qubit}} P \\ &= i\hbar\tfrac{\Omega_R}{2}(|eg\rangle\langle fg| - |fg\rangle\langle eg|) \end{aligned} \tag{1}$$

where $H = \frac{1}{2} i\hbar\Omega_R(|e\rangle\langle f| - |f\rangle\langle e|) \otimes \mathbb{1}$ is the Rabi oscillation Hamiltonian without projections. The $|eg\rangle \leftrightarrow |fg\rangle$ transition is allowed and the $|ee\rangle \leftrightarrow |fe\rangle$ transition is blocked and does not appear in the last line of Eq. (1), as shown in Fig. 1b with solid and dotted arrows, respectively. Assuming the system started in the subspace defined by P, it will remain there and undergo coherent evolution governed by $U_{\text{Zeno}} = \exp(-iH_{\text{Zeno}}t/\hbar)$. Applying the operation for a time $t = 2\pi/\Omega_R$, one full oscillation, the $|eg\rangle$ state acquires a π phase. Thus, our operation is equivalent to a Control-phase gate up to local operations. This scheme can be expanded

[1]Department of Physics, Technion - Israel Institute of Technology, Haifa, Israel. [2]Department of Physics, Harvard University, Cambridge, MA, USA. [3]Department of Chemistry, University of California, Berkeley, CA, USA. [4]Berkeley Center for Quantum Information and Computation, Berkeley, CA, USA. [5]Center for Engineered Quantum Systems, Dept. of Physics & Astronomy, Macquarie University, Sydney, NSW, Australia. ✉email: eliyab@campus.technion.ac.il

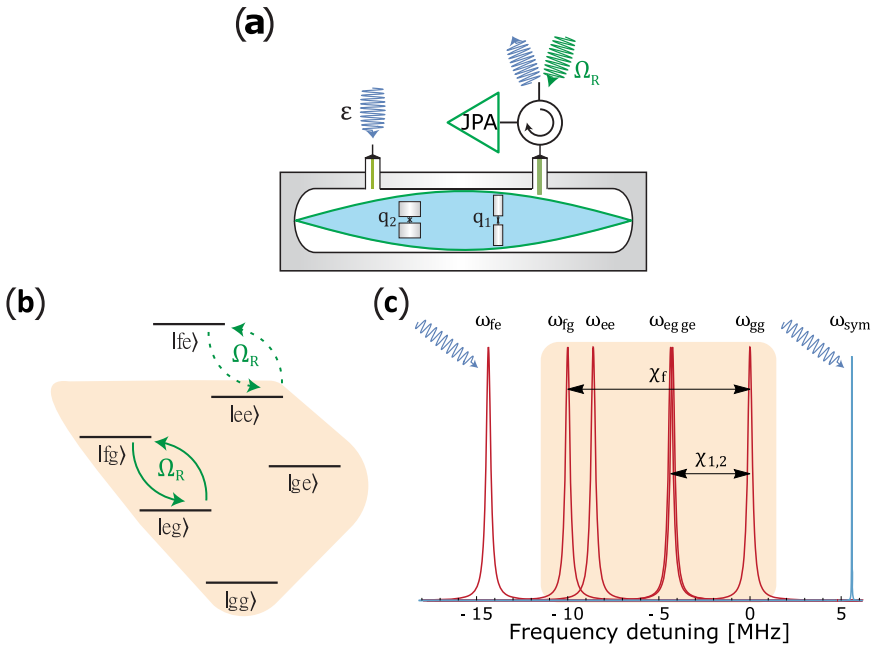

Fig. 1 Experiment schematic. a Two transmons coupled to electromagnetic-mode of a superconducting cavity. **b** Qutrit-qubit energy level diagram, where the energy levels of each element are labeled g (ground), e (excited), and f (second excited level). The colored domain is the subspace defined by the projector $P = \mathbb{1} - |fe\rangle\langle fe|$. The $|e\rangle \leftrightarrow |f\rangle$ transition of the qutrit q1 is Rabi driven with frequency Ω_R. Dotted and solid lines are blocked and allowed transitions, respectively. **c** Cavity spectra conditioned on transmon state (red) and the applied Zeno measurement drive and symmetric drive (blue).

to entangle multiple qubits and one qutrit by measuring the projector $P = \mathbb{1} - |fee...e\rangle\langle fee...e|$. A π phase will be acquired by states $|exx..x\rangle$, except for $|ee..e\rangle$, where $x \in [e, g]$. This operation is equivalent to a N-Control-phase gate. Explicitly, applying another 2π rotation between $|e\rangle \leftrightarrow |f\rangle$ of the qutrit, without the measurement tones, would impart another π phase on all states where the qutrit started in $|e\rangle$, and thus only $|ee...e\rangle$ ends up with a π phase.

The key experimental requirement is the ability to apply the projector P. In a realistic setup, the projection application rate is not infinite, and the system may be described either by a sequence of projections with a finite time interval between them, or by a continuous measurement[9]. We focus on the latter case as it fits our experimental circuit QED scheme. Evolution under Hamiltonian H combined with continuous measurements of the projector P at a rate of Γ can be modeled by the master equation

$$\frac{d\rho}{dt} = -\mathrm{i}[H, \rho] + \Gamma\mathcal{D}[P]\rho \tag{2}$$

where $\mathcal{D}[\cdot]$ is the standard Lindblad dissipator that models coupling to a Markovian bath. The finite measurement rate introduces a chance for the system to escape the Zeno subspace. The corresponding gate error in diamond norm[23] can be bounded as $\mathcal{E} < 38\ \Omega_R/\Gamma$ (see Supplementary Note 1).

Equation (2) describes the system in the Markovian regime where the bath "loses its memory" faster than the system evolution rate. This timescale puts an upper bound on the Rabi frequency Ω_R. Beyond this frequency, in the non-Markovian regime, the system cannot be described by the simple form of Eq. (2). In our system this time scale is given by the cavity linewidth κ. However, to maximize our gate fidelity, we perform the gate at a rate faster than the system decoherence, and show that Zeno dynamics are qualitatively the same, differing only in showing a limited blocking ability. This is in line with a recently predicted unification of Zeno physics arising through a wide range of mechanisms[24,25].

RESULTS

Implementation in circuit QED

We implement the Zeno gate on a circuit QED system composed of two transmons[15] dispersively coupled to a superconducting 3D cavity, Fig. 1a. The system was designed to optimize implementation of the non-local measurement P, while minimizing qubit-qutrit interactions. The transmons were fabricated with far detuned transition frequencies of $\omega_{q1}/2\pi = 3.28$ GHz, $\omega_{q2}/2\pi = 6.24$ GHz and anharmonicities of $\alpha_1/2\pi = -175$ MHz and $\alpha_2/2\pi = -225$ MHz respectively. We use $q1$ as the qutrit. The cavity mode frequency was $\omega_c/2\pi = 7.32$ GHz. The linewidth $\kappa/2\pi = 0.15$ MHz, was predominantly set by the strongly coupled port. The transmon-cavity dispersive couplings were $\chi_1/2\pi = -4.25$ MHz, $\chi_2/2\pi = -4.35$ MHz and the $|f\rangle$ state was $\chi_f/2\pi = -10$ MHz. The system–cavity interaction is well described by the dispersive Hamiltonian in the interaction picture[14]

$$H_{\mathrm{disp}}/\hbar = (\chi_1|e_1\rangle\langle e_1| + \chi_2|e_2\rangle\langle e_2| + \chi_f|f\rangle\langle f|)a^\dagger a + \alpha_1|f\rangle\langle f| \tag{3}$$

where $a^\dagger$ and a are the creation and annihilation operators of photons in the cavity, and subscripts in the kets label the qubits. We omitted the residual direct qutrit-qubit interaction, which was measured using Ramsey interferometry, between the $|ge\rangle$ and $|ee\rangle$ states and between the $|gg\rangle$ and $|eg\rangle$ states. The difference between the detunings in both cases gave ZZ interaction strength of 30 kHz, negligible for the timescales of our experiment.

Equation (3) shows that the cavity acquires a frequency shift that depends on the qutrit-qubit state. In the $|\chi| \gg \kappa$ regime, the cavity resonance frequencies for each state of the qubits are well separated, Fig. 1c. Probing the cavity resonance frequency allows us to deduce the qutrit-qubit state. We do this by driving the cavity through the weakly coupled port, and monitoring the output through the strongly coupled port. We continuously measure the projector P by driving the cavity at a frequency of $\omega_{fe} = \omega_{gg} + \chi_f + \chi_2$, which is the resonance frequency when the system is in $|fe\rangle$. We refer to such a measurement as a "Zeno drive". The output signal is amplified using a flux-pumped

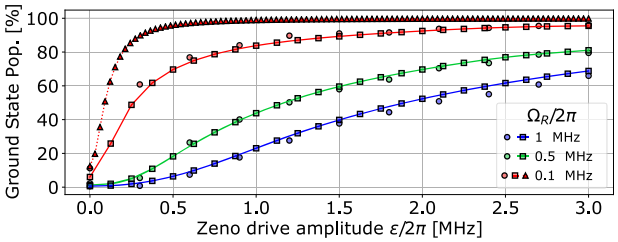

Fig. 2 Zeno blocking chance. $|gg\rangle$ population after starting in $|gg\rangle$ and Rabi driving the qutrit $|g\rangle \leftrightarrow |e\rangle$ transition for $t = \pi/\Omega_R$, while simultaneously Zeno driving the cavity at ω_{ef}, as a function of Zeno drive amplitudes ε. Circles are experimental results, squares are numerically simulated results and triangles are an ideal simulation assuming the cavity is a Markovian bath, Eq. 2 (the solid lines are provided to guide the eye).

Josephson Parametric Amplifier (JPA), with design as in[26]. Changing the pumping frequency, we sequentially amplify signals of different frequencies. We amplify the Zeno drive signal at ω_{fe} first, followed by the readout signal at ω_{gg}. The former enables us to detect whether the system escaped the Zeno subspace during the gate operation, the latter is used for tomography. We note that for the Zeno block to occur, the measurement may be performed by the "environment". High quantum efficiency is not required to implement the gate and is not even necessary to observe the measurement outcome. However, this is important for high fidelity post-selection.

Zeno blocking chance

Before proceeding to the entangling dynamics, we first characterize the Zeno block probability as a function of the drive amplitude ε. We demonstrate this here on the two lowest states of the qutrit $q1$. We apply a Zeno drive at ω_{eg} and Rabi drive the transition for $t = \pi/\Omega_R$. We measure the probability to stay in $|gg\rangle$, as a function of the Zeno drive amplitude for three different Rabi frequencies, see Fig. 2. This procedure resembles that in[27], with slight differences because that experiment was conducted using a quantum trajectory approach in the steady state. Furthermore, ref. [27] operated in the $\Omega_R < \kappa$ regime, meaning the cavity could be modeled as a Markovian bath and the textbook jump rate value of $P_{\text{jump}} = \Omega_R^2/2\Gamma$[9,28] was observed. Here we show that even beyond this regime, the Zeno effect still blocks, albeit with a reduced effectiveness.

Figure 2 shows the expected qualitative behaviour where the blocking probability increases with the drive amplitude, and decreases with increasing Rabi frequency. Quantitatively the data agree with the numerical simulation of the master equation of the full qutrit-qubit-cavity system. However, our system can be simplified to Eq. (2) only in the limit $\Omega_R \ll \kappa$. In that limit, $\Gamma = 4\varepsilon^2/\kappa$[29]. Even at $\Omega_R/2\pi = 0.1\,\text{MHz} = 2\kappa/3$ (red symbols) we can still see a deviation from Eq. (2), with a reduced blocking probability relative to that expected for this value of Γ. Recent experiments have probed pertinent regimes in greater detail[30,31], and begun to illustrate how lag in the cavity state "following" a qubit on a timescale κ^{-1} impacts subsequent measurement mediated by the cavity. While a slower Rabi frequency is better in terms of realizing the Zeno effect, our gate time needs to be significantly shorter than the system coherence times, specifically the population relaxation time T_1 and Ramsey decay time T_2^* ($T_1^{e\to g} = 52\,\mu\text{s}$, $T_1^{f\to e} = 12.9\,\mu\text{s}$, $T_2^{*e\leftrightarrow g} = 22.2\,\mu\text{s}$, $T_2^{*f\leftrightarrow e} = 5.8\,\mu\text{s}$ for the qutrit, and $T_1 = 18.9\,\mu\text{s}$, $T_2^* = 15.7\,\mu\text{s}$ for the qubit). We set $\Omega_R/2\pi = 1$ MHz (blue in Fig. 2) (see Supplementary Note 6 for a simulation of the gate with $\Omega_R/2\pi = 0.1$ MHz).

Residual effects of the Zeno drive

Until now we have discussed only the effect of the Zeno drive on the transition that we wish to block. However, residual effects on the rest of the states also emerge. Due to the non-zero cavity linewidth, driving at ω_{fe} will create a small coherent displacement even if the system is not in $|fe\rangle$. In the frame rotating with the drive frequency, at a *steady state* this coherent state is $\alpha_{ij} = \frac{\varepsilon}{i\Delta_{ij} + \kappa/2}$, where ε is the drive amplitude, and Δ_{ij} is the detuning between the cavity resonance frequency ω_{ij} and the drive frequency when the qubits are in $|ij\rangle$. In our $|\chi| \gg \kappa$ regime, we can write $\rho_{ij,k\ell}(t) = e^{i\mu_{ij,k\ell}t}\rho_{ij,k\ell}(0)$, where $\mu_{ij,k\ell} = (\omega_{ij} - \omega_{k\ell})\alpha^*_{k\ell}\alpha_{ij}$ such that a phase will be acquired between each pair of states at a rate of $\text{Re}[\mu_{ij,k\ell}] = \frac{(\omega_{ij} - \omega_{k\ell})|\varepsilon|^2}{\Delta_{ij}\Delta_{k\ell}}$ and coherence will be lost due to measurement-induced dephasing at a rate of $\text{Im}[\mu_{ij,k\ell}] = \frac{(\omega_{ij} - \omega_{k\ell})^2|\varepsilon|^2\kappa}{2\Delta_{ij}^2\Delta_{k\ell}^2}$. This is the RIP-gate, where conditional phase accumulation leads to entanglement of the qubits[18,19]. To demonstrate the entanglement caused *only* by Zeno dynamics, we negate this effect by applying an additional drive. It is applied to the cavity, at a frequency that is symmetric to the Zeno measurement drive frequency with respect to ω_{eg} and ω_{ge}, so that $\omega_{sym} = \omega_c - (\chi_f + \chi_2) + (\chi_1 + \chi_2) = \omega_c + \chi_1 - \chi_f$, as depicted in Fig. 1. This symmetric drive balances the phase accumulation, such that this no longer generates entanglement. We note that while the phase accumulation is given above for the steady state, a cancellation of the phase by the symmetric drive should also occur in the transient regime. We confirmed this by numerical simulation as well as by Ramsey interferometry between $|gg\rangle \leftrightarrow |eg\rangle$ and $|ge\rangle \leftrightarrow |ee\rangle$ while applying both the Zeno and the symmetric drives to the cavity (see Supplementary Note 3). The driven system Hamiltonian with both the Zeno drive and the symmetric drive, in the frame rotating at ω_{gg} reads

$$H_{\text{driven}}/\hbar = H_{\text{disp}}/\hbar + i\varepsilon\left(ae^{-i(\chi_f+\chi_2)t} - a^\dagger e^{i(\chi_f+\chi_2)t}\right) + i\varepsilon\left(ae^{-i(\chi_2-\chi_f)t} - a^\dagger e^{i(\chi_2-\chi_f)t}\right). \quad (4)$$

Zeno gate

To perform the Zeno gate we turn on the above drives and then initialize the system in the $(|g\rangle + |e\rangle)(|g\rangle + |e\rangle)/2$ state, see Fig. 3a (for other initial states see Supplementary Note 4). We then apply the Rabi drive $|e_1\rangle \leftrightarrow |f\rangle$ at the Stark shifted frequency for a time of $2\pi/\Omega_R$. Finally, we apply a set of tomography pulses (see Methods), and apply a readout pulse.

We sample the time evolution of the system, as shown in Fig. 3b. We see that the final state, after 1 μs, is entangled since $|eg\rangle$ has acquired a phase of π. The main discrepancy between the experiment and simulation is the population of $|fe\rangle$, which is much smaller in the experiment than in the simulation (see Supplementary Note 2 for simulation details). This is most likely due to the Zeno drive populating the cavity with a large coherent state once an escape occurs, thus shifting the qutrit resonance frequency and preventing the tomography pulse from correctly mapping $|fe\rangle$ (see Supplementary Note 4). The lost $|fe\rangle$ population is then translated to a completely mixed state, therefore increasing the computational subspace population, which can cause a calculated fidelity increase, as discussed below. In addition, the relaxation rate may be increased during the gate due to the large Zeno drive amplitude[32–35].

We performed this procedure with varying Zeno drive amplitudes and calculated the fidelity and concurrence of the final state, as shown in Fig. 4a. Since we start with the state $(|g\rangle + |e\rangle) \otimes (|g\rangle + |e\rangle)/2$ it is reasonable to use the fidelity of the final state as a proxy for the gate fidelity. As a check, we applied the gate to other initial states, obtaining similar quality results (see

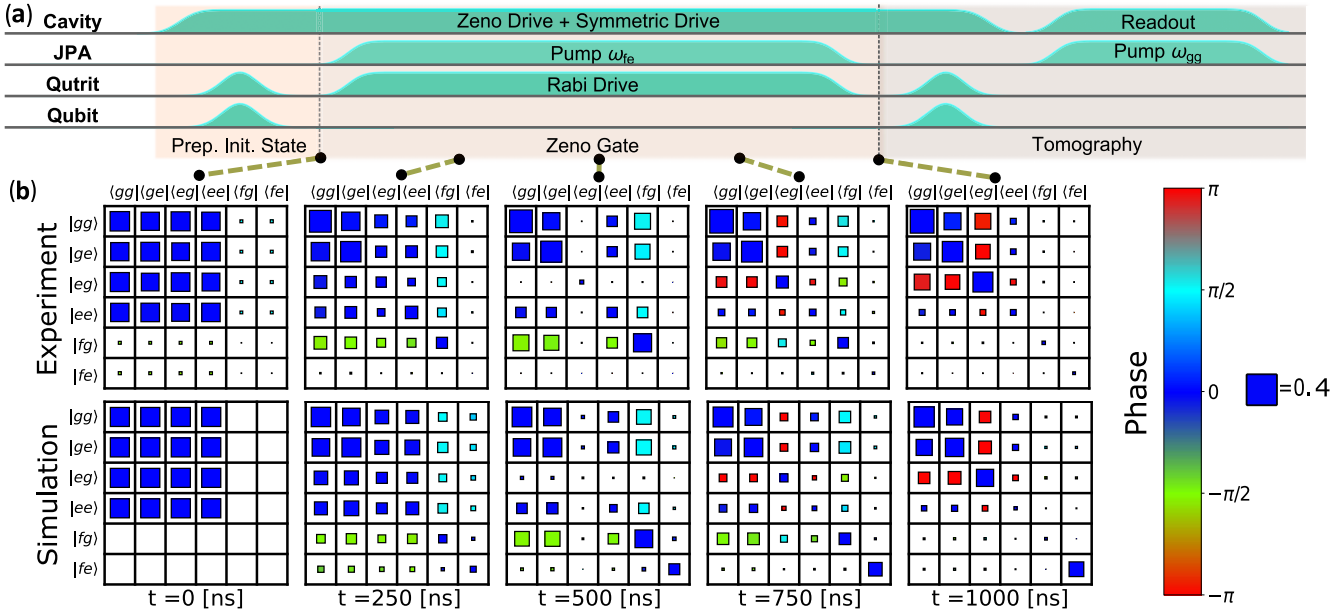

Fig. 3 Zeno gate time evolution. a Pulse sequence for the Zeno dynamics. **b** The qutrit-qubit density matrix at different times with $\varepsilon/2\pi = 2$ MHz, starting with an initial $|{+}{+}\rangle$ state, where $|+\rangle = (|g\rangle + |e\rangle)/\sqrt{2}$. Black squares are partially filled to represent the amplitude, where a full square stands for an amplitude of 0.4, and the color of the filling represents the phase according to the color bar. Experimental results (top row), numerical simulation (bottom row).

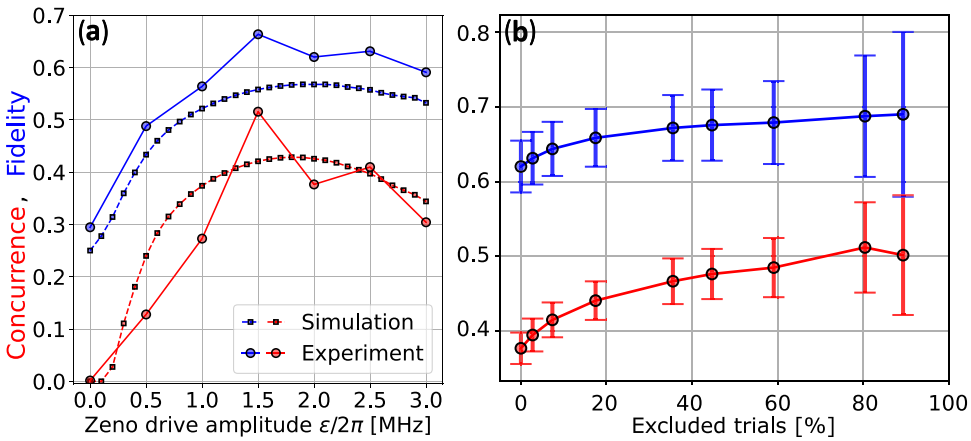

Fig. 4 Zeno gate performance. State fidelity (blue) and concurrence (red) versus the amplitude of the Zeno drive **a**, and as a function of the percentage of trials that were excluded in the post-selection procedure for a Zeno drive amplitude of 2 MHz **b**. The fidelity is calculated with respect to an ideal state, obtained by applying $\mathbb{1} - 2|eg\rangle\langle eg|$ to our initial state $|{+}{+}\rangle$. Circles are experimental results and squares are numerical results (lines are guide to the eye). The error bars in **b** represent the standard error of the means.

Supplementary Note 4). Concurrence is a measure of entanglement between qubits that is non-zero only for entangled states[36]. We calculate this on the states in the computational subspace. Increasing the Zeno drive amplitude increases the measurement rate, leading to a higher blocking probability and therefore higher fidelity and concurrence; on the other hand, this also leads to an increased dephasing rate $\mathrm{Im}[\mu_{ij,k\ell}]$, due to the finite κ. This causes the reduced fidelity and concurrence observed at higher drive amplitudes ε. Furthermore, we can see that the experimental results consistently achieve higher fidelity than the simulated results, while the experimental concurrence does not. This small discrepancy in state fidelity between the experimental results and the numerical simulation is caused primarily by the incorrect mapping of $|fe\rangle$ in the tomography process, as explained above.

The main source of infidelity for the gate is escaped from the Zeno subspace, which can be detected using the JPA. This capability allows us to perform the gate probabilistically but with a higher chance of success by post-selecting on the JPA signal. To demonstrate this, we post-selected our tomography results based on the amplitude of the transmitted signal, for the case of $\varepsilon/2\pi = 2$ MHz (see Supplementary Note 5). Figure 4b shows an increase in both state fidelity and concurrence with the percentage of excluded trials. The increase is limited by the fidelity of our error-detection, which was ~75% although our single-shot readout fidelity was ~ 93%, due to the measurement time being limited by the gate time and by the increased relaxation rate from the state $|fe\rangle$.

DISCUSSION

We have presented a system where universal control was turned on by a Zeno measurement alone. Although the measurement acts

trivially in the computational subspace, it nevertheless has a non-trivial effect on the dynamics within that subspace. To demonstrate universality, we performed an explicit gate on 2 qubits. The concept can be extended and works simultaneously on multiple qubits, under the condition that they are all coupled to the same cavity or resonator. Therefore, the number of qubits is effectively limited by frequency crowding and interqubit couplings.

To increase the fidelity of the gate, one must go further into the $|\chi| \gg \kappa$ regime. This would allow to further increase ε while keeping the measurement-induced dephasing and entangling phase accumulation rate small. However, the realistic upper bound of the dispersive coupling is 10's of MHz for current circuit QED setups.

To create an effectively non-interacting system and observe dynamics due to Zeno alone, we actively cancelled the RIP-gate mechanism. In our system, the RIP-gate alone would yield better performance for computational purposes. However, if we consider a hypothetical system with no interactions between the qubits (possibly different type of qubits) and where the measurement drive performs only the measurement with no additional entangling effect, then the Zeno will truly be the only coherent control mechanism.

Overall this experiment emphasizes the ability of the Zeno effect to turn the trivial dynamics of an apparently non-interacting system into universal control, providing proof-of-concept for measurement based, yet coherent, control strategy.

METHODS

Device parameters

The superconducting 3D cavity was made of tin plated copper, and sealed with indium. The cavity supported a TEM_{101} mode of $\omega_c/2\pi = 7.32$ GHz. The transition frequencies of the transmons were far detuned from each other and from the cavity mode in order to achieve dispersive coupling and suppress 2^{nd}-order interactions (through the cavity mode) between the transmons. In order for the dispersive coupling constant χ to be roughly equal for both transmons, q_1 was fabricated with longer pads compared with q_2. Thus, setting the dipole coupling $g_1 \approx 430$ MHz for q_1 and $g_2 \approx 110$ MHz for q_2. The transmons and JPAs were fabricated by Aluminum deposition on resist patterns formed by electron beam lithography, with a layer of ZEON ZEP 520 A resist on a layer of MicroChem 8.5 MMA EL11 resist on top of a silicon substrate. Development of the resist was done at room temperature for MMA and at 0C for ZEP. The Al/AlOx/Al Josephson junctions were fabricated using a suspended bridge fabrication process[37] for the JPAs and a bridge-free process[38] for the transmons.

We used a JPA in phase-sensitive mode to amplify the Zeno drive signal of frequency ω_{fe} by 12 dB and our readout signal of frequency ω_{gg} by 15 dB. The frequencies are separated by 14 MHz, and amplifying was enabled by changing the flux-pump frequency. The pumps were applied to the system sequentially, with a 256 ns delay, giving the JPA enough time to decay. The JPA had a 3.6 MHz bandwidth, corresponding to a single photon decay rate of $1/\kappa_{JPA} \approx 50$ ns.

The full system schematics are described in Supplementary Fig. 1.

Tomography details

To perform full state tomography, we measure all the operators that span the Hilbert space, which is a total of 36 operators for a qutrit and a qubit. We partially map each operator to the projector that we measure $|gg\rangle\langle gg|$, as was done in[39]. We then acquire the expectation value of each of the 36 operators. To reconstruct the density matrix, we use a method of maximum likelihood estimation (MLE) as described in ref. [40] to find the most likely valid density matrix. If the trace of the density matrix is less than 1, the MLE process will effectively add an appropriately scaled completely mixed state to achieve $\mathrm{Tr}[\rho] = 1$.

DATA AVAILABILITY

The data that support the findings of this study are available from the corresponding author upon reasonable request.

CODE AVAILABILITY

The code that supports the findings of this study are available from the corresponding author upon reasonable request.

Received: 8 December 2021; Accepted: 27 June 2022;
Published online: 25 July 2022

REFERENCES

1. Motzoi, F., Whaley, K. B. & Sarovar, M. Continuous joint measurement and entanglement of qubits in remote cavities. *Phys. Rev. A* **92**, 032308 (2015).
2. Martin, L., Motzoi, F., Li, H., Sarovar, M. & Whaley, K. B. Deterministic generation of remote entanglement with active quantum feedback. *Phys. Rev. A* **92**, 062321 (2015).
3. Thomsen, L., Mancini, S. & Wiseman, H. M. Continuous quantum nondemolition feedback and unconditional atomic spin squeezing. *J. Phys. B* **35**, 4937 (2002).
4. Jacobs, K. How to project qubits faster using quantum feedback. *Phys. Rev. A* **67**, 030301 (2003).
5. Riste, D. et al. Deterministic entanglement of superconducting qubits by parity measurement and feedback. *Nature* **502**, 350–354 (2013).
6. Katz, N. et al. Reversal of the weak measurement of a quantum state in a superconducting phase qubit. *Phys. Rev. Lett.* **101**, 200401 (2008).
7. Vool, U. et al. Continuous quantum nondemolition measurement of the transverse component of a qubit. *Phys. Rev. Lett.* **117**, 133601 (2016).
8. Hacohen-Gourgy, S. & Martin, L. S. Continuous measurements for control of superconducting quantum circuits. *Adv. Phys.-X* **5**, 1813626 (2020).
9. Facchi, P. & Pascazio, S. Quantum zeno dynamics: mathematical and physical aspects. *J. Phys. A* **41**, 493001 (2008).
10. Burgarth, D. et al. Exponential rise of dynamical complexity in quantum computing through projections. *Nat. Commun.* **5**, 5173 (2014).
11. Wang, X.-B., You, J. Q. & Nori, F. Quantum entanglement via two-qubit quantum zeno dynamics. *Phys. Rev. A* **77**, 062339 (2008).
12. Shao, X.-Q., Wang, H.-F., Chen, L., Zhang, S. & Yeon, K.-H. One-step implementation of the toffoli gate via quantum zeno dynamics. *Phys. Lett. A* **374**, 28–33 (2009).
13. Zhang, S., Shao, X.-Q., Chen, L., Zhao, Y.-F. & Yeon, K.-H. Robust $\sqrt{swap}$ gate on nitrogen-vacancy centres via quantum zeno dynamics. *J. Phys. B* **44**, 075505 (2011).
14. Blais, A., Grimsmo, A. L., Girvin, S. M. & Wallraff, A. Circuit quantum electrodynamics. *Rev. Mod. Phys.* **93**, 025005 (2021).
15. Koch, J. et al. Charge-insensitive qubit design derived from the cooper pair box. *Phys. Rev. A* **76**, 042319 (2007).
16. Roch, N. et al. Observation of measurement-induced entanglement and quantum trajectories of remote superconducting qubits. *Phys. Rev. Lett.* **112**, 170501 (2014).
17. Shankar, S. et al. Autonomously stabilized entanglement between two superconducting quantum bits. *Nature* **504**, 419–422 (2013).
18. Cross, A. W. & Gambetta, J. M. Optimized pulse shapes for a resonator-induced phase gate. *Phys. Rev. A* **91**, 032325 (2015).
19. Paik, H. et al. Experimental demonstration of a resonator-induced phase gate in a multiqubit circuit-qed system. *Phys. Rev. Lett.* **117**, 250502 (2016).
20. Isenhower, L. et al. Demonstration of a neutral atom controlled-not quantum gate. *Phys. Rev. Lett.* **104**, 010503 (2010).
21. Levine, H. et al. Parallel implementation of high-fidelity multiqubit gates with neutral atoms. *Phys. Rev. Lett.* **123**, 170503 (2019).
22. Jaksch, D. et al. Fast quantum gates for neutral atoms. *Phys. Rev. Lett.* **85**, 2208–2211 (2000).
23. Watrous. The Theory of Quantum Information (Cambridge university press, 2018).
24. Burgarth, D. et al. Generalized adiabatic theorem and strong-coupling limits. *Quantum* **3**, 152 (2019).
25. Burgarth, D. et al. Quantum zeno dynamics from general quantum operations. *Quantum* **4**, 289 (2020).
26. Hacohen-Gourgy, S. et al. Quantum dynamics of simultaneously measured noncommuting observables. *Nature* **538**, 491–494 (2016).
27. Slichter, D. H. et al. Quantum zeno effect in the strong measurement regime of circuit quantum electrodynamics. *N. J. Phys.* **18**, 053031 (2016).
28. Misra, B. & Sudarshan, E. C. G. The zeno's paradox in quantum theory. *J. Math. Phys.* **18**, 756–763 (1977).
29. Gambetta, J. et al. Quantum trajectory approach to circuit qed: Quantum jumps and the zeno effect. *Phys. Rev. A* **77**, 012112 (2008).
30. Szombati, D. et al. Quantum rifling: Protecting a qubit from measurement back action. *Phys. Rev. Lett.* **124**, 070401 (2020).
31. Koolstra, G. et al. Monitoring fast superconducting qubit dynamics using a neural network. Preprint at https://arxiv.org/abs/2108.12023 (2021).

32. Slichter, D. H. et al. Measurement-induced qubit state mixing in circuit qed from up-converted dephasing noise. *Phys. Rev. Lett.* **109**, 153601 (2012).
33. Sank, D. et al. Measurement-induced state transitions in a superconducting qubit: Beyond the rotating wave approximation. *Phys. Rev. Lett.* **117**, 190503 (2016).
34. Hanai, R., McDonald, A. & Clerk, A. Intrinsic mechanisms for drive-dependent purcell decay in superconducting quantum circuits. *Phys. Rev. Res.* **3**, 043228 (2021).
35. Lescanne, R. et al. Escape of a driven quantum josephson circuit into unconfined states. *Phys. Rev. Appl.* **11**, 014030 (2019).
36. Wootters, W. K. Entanglement of formation of an arbitrary state of two qubits. *Phys. Rev. Lett.* **80**, 2245–2248 (1998).
37. Yeh, J. T. C. Technique for fabrication of superconducting microbridges and small josephson tunnel junctions. *J. Appl. Phys.* **45**, 4617–4621 (1974).
38. Zhang, K., Li, M.-M., Liu, Q., Yu, H.-F. & Yu, Y. Bridge-free fabrication process for al/AlOx/al josephson junctions. *Chin. Phys. B* **26**, 078501 (2017).
39. Reed, M. D. Entanglement and Quantum Error Correction with Superconducting Qubits. Ph.D. thesis, (2014).
40. Singh, H., Arvind, & Dorai, K. Constructing valid density matrices on an nmr quantum information processor via maximum likelihood estimation. *Phys. Lett. A* **380**, 3051–3056 (2016).

ACKNOWLEDGEMENTS

This research was supported by ISF Grant no. 1113/19, US-Israel BSF Grant no. 2020166, and Technion's Helen Diller Quantum Center. P.L. and K.B.W. were partially supported by the U.S. Department of Energy, Office of Science, National Quantum Information Science Research Centers, Quantum Systems Accelerator. D.B. acknowledges funding by the ARC (Project numbers FT190100106, DP210101367, CE170100009).

AUTHOR CONTRIBUTIONS

D.B., L.S.M., and S.H.-G. conceived the study. The device was fabricated by C.M. and A.A.D. E.B. and A.A.D. constructed the experimental setup. The experiment and data analysis was done by E.B., assisted by A.A.D. Theoretical modeling was done by L.S.M., S.H.-G., D.B., E.B., and P.L. E.B. and S.H.-G. wrote the manuscript. All authors contributed to the discussions and preparation of the manuscript. All work was carried out under the supervision of S.H.-G. and K.B.W.

COMPETING INTERESTS

The authors declare no competing interests.

ADDITIONAL INFORMATION

Supplementary information The online version contains supplementary material available at https://doi.org/10.1038/s41534-022-00594-4.

Correspondence and requests for materials should be addressed to E. Blumenthal.

Reprints and permission information is available at http://www.nature.com/reprints

Publisher's note Springer Nature remains neutral with regard to jurisdictional claims in published maps and institutional affiliations.